Title

Pliocene-Pleistocene initiation, style, and sequencing of deformation in the central Tien Shan

Journal

Tectonics, 33(4)

ISSN

0278-7407

Authors

Goode, Joseph K
Burbank, Douglas W
Ormukov, Cholponbek

Publication Date

2014-04-01

DOI

10.1002/2013tc003394

Peer reviewed

AGU PUBLICATIONS

Tectonics

RESEARCH ARTICLE
10.1002/2013TC003394

Key Points:
- Dates of folded terraces constrain structure timing
- Geologic and geodetic deformation rates are consistent
- Naryn basin structures originated about 1 Ma

Correspondence to:
J. K. Goode,
jgoode@eri.ucsb.edu

Citation:
Goode, J. K., D. W. Burbank, and C. Ormukov (2014), Pliocene-Pleistocene initiation, style, and sequencing of deformation in the central Tien Shan, *Tectonics*, *33*, 464-484, doi:10.1002/2013TC003394.

Received 7 JUN 2013
Accepted 4 MAR 2014
Accepted article online 13 MAR 2014
Published online 11 APR 2014

Pliocene-Pleistocene initiation, style, and sequencing of deformation in the central Tien Shan

Joseph K. Goode[1], Douglas W. Burbank[1], and Cholponbek Ormukov[2]

[1]Department of Earth Science, University of California, Santa Barbara, California, USA, [2]Central-Asian Institute for Applied Geoscience, Bishkek, Kyrgyzstan

Abstract In response to the Indo-Asian collision, deformation of the Tien Shan initiated at ~25 Ma along the northwestern margin of the Tarim Basin. 300 km north, the Kyrgyz Range began deforming ~15 Ma later. Although multiple intervening structures across the Tien Shan are currently active, the sequencing of initial deformation across the orogen's entire width remains poorly known. To determine whether deformation migrated sequentially northward or developed less predictably, we documented deformation patterns within the Naryn Basin in south-central Kyrgyzstan. Detailed mapping and a published balanced cross section across the Naryn Basin suggest that deep-seated, relatively steeply dipping thrust faults have disrupted the basin during late Cenozoic deformation. Dating of deformed fluvial terraces with ages between ~10 and 250 ka constrains the rate of deformation across relatively young structures in the Tien Shan interior. Based on geodetic surveys of dated terraces, local rates of relative rock uplift span from 0.3 to 3.5 mm/yr. Folding rates and patterns are temporally persistent at a given site. Moreover, they mimic modern geodetic rates measured from interferometric synthetic aperture radar. Extrapolating these rates into the past suggests that structures within the interior of the Naryn Basin formed in the last 1 Myr, whereas the ranges surrounding the basin initiated at least 1–4 Myr earlier. Hence, within the Naryn Basin itself, deformation has migrated from margins to interior. Similarly, these new chronologies indicate that at least some deformation in the interior of the Tien Shan initiated millions of years later than along either orogenic margin.

1. Introduction

The Tien Shan comprise a suite of bedrock ranges 3 to 4 km in height that rise above intervening, sediment-filled basins. Thermochronologic and paleomagnetic studies have been used to measure the expansion of the central Tien Shan as individual ranges have begun to grow through time [*Abdrakhmatov et al*., 2001; *Bullen et al*., 2003; *Glorie et al*., 2010; *Heermance et al*., 2007; *Sobel et al*., 2006a, 2006b]. As a result of this work, a sequence of orogenic growth has begun to emerge (Figure 1). The oldest range of the central Tien Shan (74–75° longitude) lies in the hanging wall of the Maidan thrust in China where the onset of rapid cooling is dated at 24 Ma [*Sobel et al*., 2006a] and is nearly synchronous with the onset of coarse deposition in the nearby, northwestern Tarim foreland [*Yin et al*., 1998]. Younger contractional structures are found to both the north and south, but the greater extent of the central Tien Shan lies to the north in Kyrgyzstan. The Kyrgyz Range, which defines the northern limit of the central Tien Shan, began to deform ~12–11 Ma [*Bullen et al*., 2001, 2003]. Although *Abdrakhmatov et al.* [2001] used estimated stratigraphic ages to suggest that many individual ranges of the Kyrgyz Tien Shan may have initiated ~12–13 Ma, the only well-established dates for the onset of late Cenozoic exhumation permit sequential migration of deformation across the Kyrgyz Tien Shan from south to north between 24 and 11 Ma (Figure 1) [*Bullen et al*., 2003; *Dumitru et al*., 2001; *Glorie et al*., 2010; *Macaulay et al*., 2013; *Sobel et al*., 2008]. Given the uncertain initiation ages within central Kyrgyzstan, the migration of deformation could be progressive in a steady or a highly pulsed mode, or it could be nonsystematic or random.

Even though the expansion of the Tien Shan to its present northern limit occurred ~10 Ma, current deformation is distributed across the entire breadth of the central Tien Shan as demonstrated by seismicity [*Ghose et al*., 1998; *Mellors et al*., 1997; *Molnar and Ghose*, 2000], geodesy [*Reigber et al*., 2001; *Abdrakhmatov et al*., 1996; *Zubovich et al*., 2010], and late Quaternary deformation [*Thompson et al*., 2002]. The most rapid Quaternary shortening is found within the Naryn Basin [*Thompson et al*., 2002]. From ridge crest to ridge crest, the Naryn Basin spans 65 km, or about 20%, of the 350 km north-to-south width of the central Tien Shan

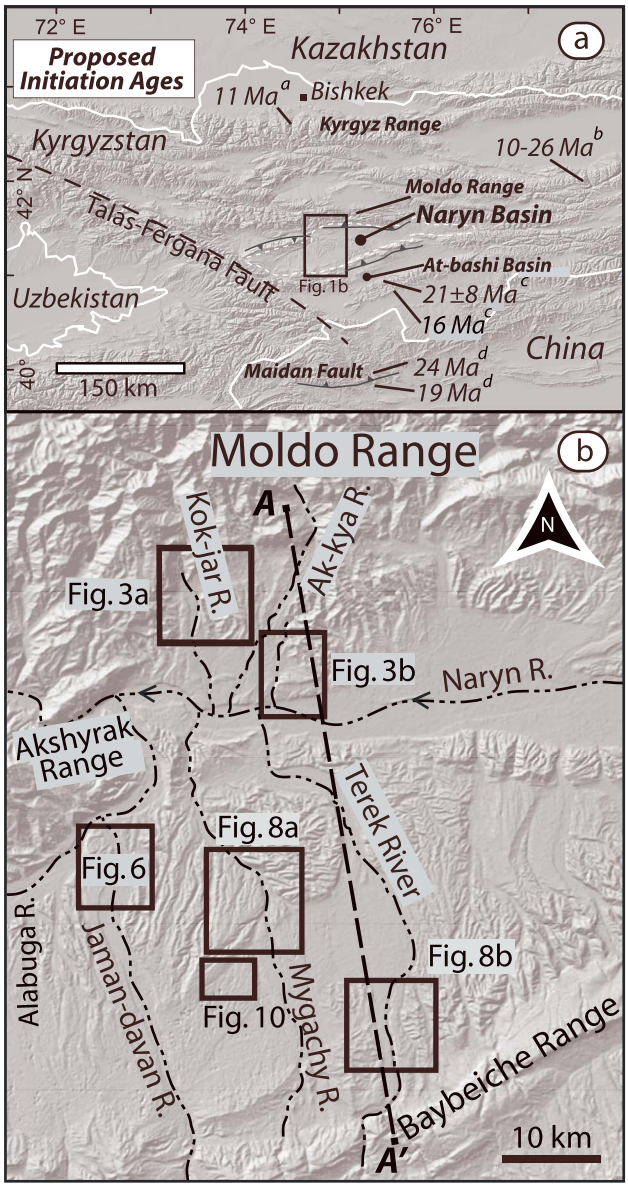

Figure 1. (a) Shaded relief map of the central Tien Shan. Estimates of the initiation for several ranges are based on thermochronometry. Superscripts refer to publication of age control: *a* is *Bullen et al.* [2003] and *Sobel et al.* [2008], *b* is *Macaulay et al.* [2013], *c* is *Sobel* [1999], and *d* is *Dumitru et al.* [2001] and *Sobel et al.* [2006a]. The western Naryn Basin (area in box) is the focus of this study. (b) Western Naryn Basin. Detailed maps from the boxed regions in subsequent figures show terraces along five tributaries of the Naryn River. Cross section along A-A' is shown in Figure 14.

(Figure 1). The western Naryn Basin was divided from the neighboring At-Bashi Basin by the growth of reverse-faulted Baybeiche Range that now forms the southern Naryn Basin margin [*Burbank et al.*, 1999]. The Moldo Range on the Naryn Basin's northern margin separates it from the Son-Kul Basin. Sequential expansion of the orogen from south to north implies that the structures in the Naryn Basin region would have initiated between 24 and 11 Ma. Thus, new estimates of the onset of deformation across the Naryn Basin can help constrain the timing and style of growth of the Kyrgyz Tien Shan, test conceptual models for the sequencing of deformation across the entire Tien Shan, and provide insights on the evolutionary patterns of contractional orogens comprising a suite of ranges and intramontane basins.

Although the topographic expression of the Tien Shan is dominated by the high relief of bedrock ranges, currently active tectonic structures are commonly found within Cenozoic Basins rather than directly adjacent to the bedrock ranges [*Bullen et al.*, 2003; *Burbank et al.*, 1999; *Heermance et al.*, 2007; *Hubert-Ferrari et al.*, 2007; *Tapponnier and Molnar*, 1979; *Thompson et al.*, 2002] . The sedimentary formations within intramontane basins are less resistant to erosion and do not support the striking relief of the surrounding ranges, but they do record the Tien Shan's growth. Within one such intramontane basin, the Naryn Basin, active faults, and folds commonly deform both Cenozoic strata and younger, Quaternary fluvial terraces. Additionally, this deformation disrupts modern fluvial networks that traverse the basin [*Burbank et al.*, 1999].

This study describes rates of deformation and structural geometries of a suite of Cenozoic fault-related folds situated in the Naryn Basin. These contractional structures dissect the broad western portion of the Naryn Basin and lie west of the folded terraces studied by *Thompson and others* [2002]. Rates are calculated from topographic surveys of folded river terraces that are combined with dates of terrace-top deposits. We compare the calculated rates, which represent average rates over the last 10–250 kyr, to modern geodetic deformation rates measured with interferometric synthetic aperture radar (InSAR) [*Goode et al.*, 2011]. This comparison reveals that both the rates and loci of deformation across the western Naryn Basin appear remarkably consistent between the present day and middle to late Quaternary times. Thus, we show that multiple folds have grown and continue

to grow simultaneously. Extrapolation of these local, apparently steady rates into the past allows us to estimate when these structures first became active. In addition, these estimates for the initiation of deformation provide key constraints on the spatial pattern of deformation. They show that, as is typical of foreland fold-and-thrust belts, deformation propagated sequentially into the adjacent basin. In contrast, the initiation ages for the bedrock ranges bounding the Naryn Basin indicate that at least some of the range-scale deformation within the Tien Shan significantly postdates range growth on either margin of the orogen and argues for large-scale, out-of-sequence deformation in Plio-Pleistocene times.

2. Western Tien Shan and Naryn Basin Geology

A regionally extensive unconformity underlies the 3 to 4 km thick Cenozoic strata of the Kyrgyz Tien Shan [*Burbank et al*., 1999; *Cobbold et al*., 1996; *Oskin and Burbank*, 2007]. This unconformity is beveled across previously deformed units that generally record the amalgamation of the central Asian continent during Paleozoic time [*Burtman*, 1975; *Sengor and Natal'in*, 1996; *Windley et al*., 2007]. Two red-hued, Cenozoic terrestrial sedimentary units, the Kokturpak and Shamsi formations, are found directly overlying the unconformity in the Naryn and other intramontane basins of the Kyrgyz Tien Shan [*Abdrakhmatov et al*., 2001; *Makarov*, 1977; *Chediya*, 1986]. Across extensive exposures, the parallelism of overlying Cenozoic strata with the unconformity indicates the presence of low relief on the unconformity at the time of its burial [*Omuraliev*, 1978]. The basal Kokturpak formation comprises residual conglomeratic lags, marls, and paleosols that attain aggregate thicknesses of 0 to 130 m along the length of the Naryn Basin. The overlying, sandstone-dominated Shamsi Formation thickness varies from 200 to 800 m across the length of the Naryn Basin. Overlying the Shamsi, the Chu Formation comprises gray-green fluvial-lacustrine sand and siltstone. Measurements of Chu thickness preserved in the Naryn Basin vary between 2 and 3.2 km [*Makarov*, 1977; *Omuraliev*, 1978]. Measured stratigraphic sections are restricted to exposures along the uplifted margins of the basin. Cenozoic deformation and erosion has exposed resistant units into which the regional unconformity was beveled. This exhumed surface, therefore, serves as a regional strain marker where it is preserved across the uplifted basin-bounding ranges.

Locally derived conglomerates that primarily comprise limestone clasts commonly occur along the basin margins. This unit, the Sharpyldak Formation, overlies and interfingers with the finer-grained Chu Formation. Additionally, gravel and cobble conglomerates form Quaternary terrace-top deposits that rest unconformably on river-cut strath surfaces. The clast composition of these terraces reflects the bed load of the contributing rivers, some of which carry distinctive lithologies. For example, terrace conglomerates deposited by the Naryn River commonly contain pink-colored intrusive igneous clasts, whereas terraces formed by tributary rivers draining the surrounding ranges are dominated by dark limestone with rare quartzite clasts. Thus, even though the positions of the river systems have shifted through time, abandoned terrace levels can commonly be genetically linked to either the modern Naryn River or one of its tributaries.

The youngest accumulation of sediment in the Naryn Basin is a white silt and clay lacustrine fill. The western Naryn Basin is locally known as "Ak Talaa" meaning white ground due to the prominence of this sedimentary unit. These sediments are interpreted to have accumulated in a landslide-dammed lake upstream of the Besh-kol landslide [*Strom and Korup*, 2006]. Benches on hillsides rising above the fill level preserve ancient shoreline berms. Although the top of this lacustrine fill could serve as an additional strain marker, no deformation of this surface was documented in this study.

3. Methods

3.1. Deformation Measurement

Folded Cenozoic strata within the Naryn Basin record deformation accommodated in the basin since their deposition. Abandoned fluvial terrace surfaces that were either beveled across these Cenozoic units or deposited atop them now serve as strain markers recording deformation since terrace abandonment. We surveyed terrace profiles across structures within the basin using decimeter-scale precision handheld differential GPS units (*Trimble Geo XH*) in order to quantify the postabandonment terrace deformation. Survey data were corrected with respect to a stationary GPS receiver. For each surveyed structure, we also recorded bedding attitudes from nearby outcrops.

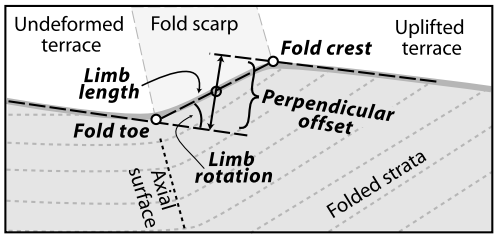

Figure 2. Terrace deformation can be measured in terms of the dip of the fold limb, the length of the tilted fold limb, and the perpendicular offset. Linear regressions through survey profiles facilitate calculation of these metrics and the identification of hinge points at the toe and crest of the fold.

From surveyed profiles, we calculate several metrics of deformation (Figure 2). Generally, the terrace limb dip is measured with respect to the gently sloping terrace below the fold toe rather than with respect to a horizontal datum. Similarly, the distance that a terrace is offset by a fold scarp is measured perpendicular to the average gradient of the upper and lower planar portions of the folded surface. Given that undeformed terrace surfaces generally have dips of less than 2°, the terrace-perpendicular offset will be only slightly different than the vertical separation of the same terrace across the same fold scarp. The length of the tilted limb can be measured from crest to toe. Measuring limb length requires location of points defining the crest and toe of the fold in cross section. These fold vertices are commonly not well preserved because of the combined effects of erosion from the crest of the fold limb, deposition at the toe of the fold, and the presence of rounded rather than perfectly angular fold hinges. Instead, the intersection points between lines that have been fit through the survey data define the virtual kinks near the rounded toe and crest. At one locality, the entire length of preserved terrace is warped. In this case, we estimate the original terrace gradient from the shape of the modern drainage profile.

Uncertainties in each measure of deformation (angle, length, and offset) are simulated and combined with a Monte Carlo approach [*Thompson et al.*, 2002]. Least squares regression through survey points defining planar fold limbs provides best fit linear parameters and associated uncertainties. A normally distributed population with the same mean and variance is generated and sampled with 10^4 synthetic data points for each parameter. The reported terrace offset across each structure represents the mean and 1 standard deviation uncertainty of 10^4 calculations of deformation metrics from these synthetic values. Similarly, rates of deformation are calculated based on the distribution of probable ages, and uncertainties of 1 standard deviation are reported. For calibrated radiocarbon ages, this distribution is not Gaussian.

3.2. Dating of River Terraces

At six localities in the western Naryn Basin, we collected rock samples for age determination by optically stimulated luminescence (OSL) [*Duller*, 1996; *Huntley et al.*, 1985] using the single-aliquot, regenerative-dose method [*Murray and Wintle*, 2000, 2003]. These analyses were performed by the University of Gloucestershire Geochronology Laboratories. We collected ~1 kg blocks of sedimentary rock near the top of the terrace fill above an underlying strath surface. Although limestone cobble conglomerates dominate most of these terrace-capping deposits, rare silt or fine sand beds from 30 to 60 cm thick were targeted for sampling. All resulting OSL ages are considered tentative as a result of overdispersed regenerative-dose data [*Galbraith*, 1990] and because dose rates were determined from block samples in the laboratory rather than in situ. Because fluvial terraces begin to record deformation after abandonment, these ages place an upper limit on the age of terrace abandonment and a lower limit on rates of deformation calculated from them.

Charcoal samples from three localities were dated in an accelerator mass spectrometer (AMS) based on C^{14} content. Two of these samples were paired with OSL samples. Radiocarbon ages were calibrated to calendar years before present using OxCal software [*Ramsey*, 2009] and the IntCal 09 calibration curves [*Reimer et al.*, 2009]. All age determinations are summarized in Tables 1 and 2.

In addition to the analytic uncertainties associated with geochronology, geologic complexity can confound or mislead the interpretation of the results. Where active faults or folds disrupt a terrace, terrace abandonment may have been caused by a combination of tectonic and hydrologic drivers, thus complicating the timing of abandonment. Additionally, younger terraces may be cut into older terrace deposits such that the provenance of a particular terrace-top sample may be unclear. Finally, active fold growth on the downstream reaches of a terrace can cause ponding of younger sediments on top of the formerly abandoned terrace surface.

AGU Tectonics

10.1002/2013TC003394

Table 1. Summary of Dated OSL Samples

Sample Name	Age (ka)	Uncertainty (±1σ)	Dose Rate (Gy/ka)	Latitude (°N)	Longitude (°E)	Elevation (m)	Depth (m)	Description (From Surface Downward)	
Akchiy 100902 OSLA	593[a]	50	2.63 ± 0.08	41.21	74.816	2067	2	Ground Surface; 2 m limestone-dominated gravel/cobble conglomerate; 30 cm silt bed (sample horizon); >10 m limestone cobble conglomerate	High Mygachy River surface
Akchiy 100902 OSLB	175[b]	13	2.16 ± 0.10	41.21	74.816	2067	2	Ground Surface; 2 m limestone-dominated gravel/cobble conglomerate; 30 cm silt bed (sample horizon); >10 m limestone cobble conglomerate	Duplicate from high Mygachy River surface
Bad Pass 100905 OSLD	121[c]	17	2.39 ± 0.11	41.27	74.668	1867	8	Ground Surface; 8 m limestone-dominated gravel/cobble conglomerate; 30 cm silt bed (sample horizon); >10 m limestone cobble conglomerate	Jaman-davan River surface
Cemetery 100905 OSLA	66[b]	9	2.25 ± 0.10	41.22	74.849	2000	1	Ground Surface; 0.5 m loess; 0.25 m limestone-dominated gravel/cobble conglomerate; 60 cm silt bed (sample horizon); >5 m limestone cobble conglomerate	Low Mygachy River surface; OSL and charcoal sample
S Ak-kya 100831 OSLA	270[a]	17	2.60 ± 0.08	41.46	74.868	1780	2	Ground Surface; 1.5 m limestone-dominated gravel/cobble conglomerate; 20 cm silt bed (sample horizon); 3 m limestone cobble conglomerate; Underlying sand-siltstone formation	High Ak-kya Valley surface
Karakou 100901 OSLB	13[b]	1	2.02 ± 0.06	41.47	74.77	1784	4	Ground Surface; 4 m limestone-dominated gravel/cobble conglomerate; 15 cm silt bed (sample horizon); >10 m limestone cobble conglomerate	High Kok-jar River surface
Karakou 100901 OSLC	14[b]	1	1.76 ± 0.06	41.46	74.78	1770	1.4	Ground Surface; 1.4 m limestone-dominated gravel/cobble conglomerate; 40 cm silt bed (sample horizon); >10 m limestone cobble conglomerate	Low Kok-jar River surface; OSL and charcoal sample

[a]Accept as minimum age with strong reservations.
[b]Accept tentatively.
[c]Accept tentatively as minimum age.

Table 2. Summary of Radiocarbon Ages From Charcoal Samples

Sample Name	C^{14} Age	±(1σ)	Calibrated Age	±(1σ)	Latitude (°N)	Longitude (°E)	Elevation (m)	Depth (m)	Description
Cemetery 100905[a]	39.50 ka	1.2 ka	43.8 ka	0.9 ka	41.22	74.849	2000	1	Low Mygachy River surface; OSL and charcoal sample
Karakou 100901[a]	5.32 ka	.05 ka	6.10 ka	.077 ka	41.46	74.780	1770	1.4	Low Kok-Jar River surface; OSL and charcoal sample
SR09C[b]	1430	40	1430	55	41.383	75.166	1801	1.6	Silt fill in Snake River Valley (Naryn Lake)

[a]Analysis performed by Arizona AMS Facility, University of Arizona Physics Department.
[b]Analysis performed by Beta Analytic Inc.

3.3. Modern Geodetic Deformation Rates

Satellite-based interferometric synthetic aperture radar (InSAR) provides a sensitive measure of near-vertical displacements of the ground surface [*Burgmann et al.*, 2000; *Massonnet et al.*, 1993]. These data may represent the motion of the ground surface toward or away from a satellite between repeated image acquisitions as interseismic strain accumulates over the course of several years. By comparing phase changes between radar images, differences in radar line-of-sight distance can be measured at the millimeter scale. A map of ground surface displacements along the satellite line of sight across the Naryn Basin was generated from 10 individual radar images spanning acquisition times between October 2003 and June 2009 [*Goode et al.*, 2011]. We use a subset of those data covering the western Naryn Basin to compare Quaternary and modern deformation rates.

Similar to previous studies of structural initiation across the central Tien Shan [*Dumitru et al.*, 2001; *Glorie et al.*, 2010; *Sobel et al.*, 2008], untested assumptions underlie the estimates presented here. We assume both that surficial geologic mapping of the structures adequately constrains the total deformation across the structures and that rates based on Quaternary ages presented in this study have remained constant through time, such that we can calculate an initiation age for each structure.

4. Results

A suite of folds dissects the western Naryn Basin. These structures and associated terraces are described beginning in the north and moving sequentially toward the south. At each locality, deformed terraces record some fraction of the total deformation accommodated by the structure. Terrace levels are labeled according to the associated modern river and their relative elevation above the modern drainage. For example, "High Kok-jar terrace" describes the highest terrace preserved above the Kok-Jar River. Importantly, the highest terrace associated with one drainage is not necessarily coeval with a similarly high terrace cut by another river. Folded terrace limb lengths, offsets, and angles are summarized in Table 3.

Table 3. Summary of Deformation Measured From Deformed Terraces

Terrace Locality	Terrace Level	Terrace Slope[a] (° ± 1σ)	Limb Length (m ± 1σ)	Perpendicular Offset[b] (m ± 1σ)	Terrace Age (ka ± 1σ)	Perpendicular Offset Rate (mm/yr ± 1σ)
Kok-Jar terraces	Remnant	—	—	80 ± 1	—	—
	High	—	—	51 ± 1	13 ± 1	3.9 ± 0.4
	Low	—	—	20 ± 1	6 ± 0.1	3.3 ± 0.1
Ak-kya terraces	High	14	—	>190	270 ± 17	>0.7 ± 0.1
	Middle inset	5	—	—	—	—
	Low inset	4	—	—	—	—
Jaman-davan terraces	High	19	180 ± 2	85 ± 1	121 ± 17	0.7 ± 0.1
	Middle	12	144 ± 4	39 ± 1	—	—
	Low	23	31 ± 1	18 ± 1	—	—
Mygachy terraces	High	21	223 ± 5	87 ± 2	175 ± 13	0.5 ± 0.04
	Low	9	190 ± 3	32 ± 1	66 ± 9	0.5 ± 0.1
Terek terraces	High	10	386 ± 5	41 ± 1	55 ± 8[c]	0.8 ± 0.1[c]
	Low	5	574 ± 14	17 ± 1	25 ± 3[c]	0.7 ± 0.1[c]

[a]Fold scarp slope measured following Figure 2.
[b]Fold scarp length measured following Figure 2.
[c]Terek terrace ages and rates are based on tentative correlation to Jaman-davan terraces.

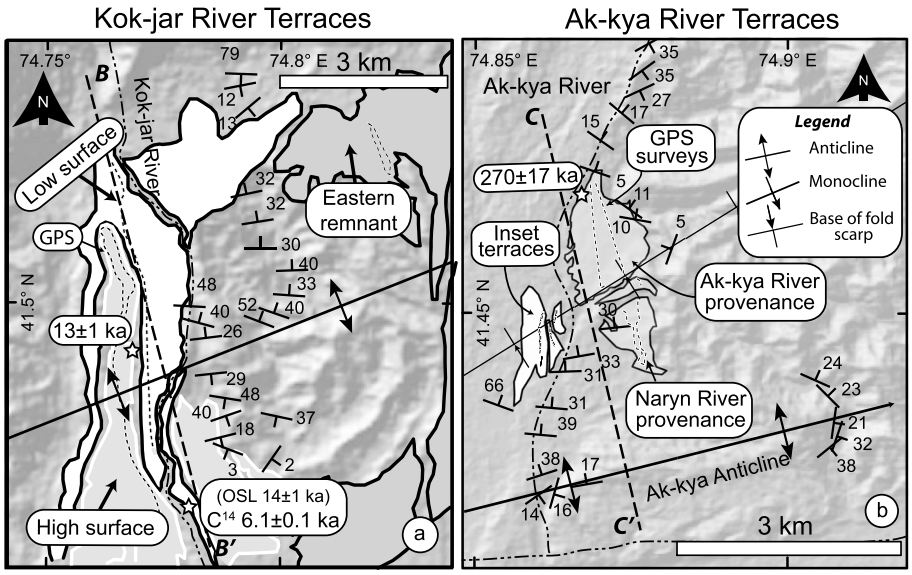

Figure 3. (a) Terraces along the Kok-jar River (see Figure 1b for location). Stars mark locations of four dated samples. (Ages that we deem less reliable are shown in parentheses.) Survey paths (dashed lines) show location of GPS surveys plotted in Figure 4b. (b) Folded fluvial terraces in the vicinity of the Ak-kya River (see Figure 1b for location). The upper terrace (dark gray) records folding in the north limb of a broad anticline truncated by the Naryn River. Deposits at the southern end of the high surface indicate Naryn River provenance. Inset surfaces (light gray) record later folding. Dashed lines show locations of differential GPS surveys plotted in Figure 5b. White stars show locations of dated samples.

We dated a total of 10 samples from terrace levels preserved in the Naryn Basin using either OSL or radiocarbon (Tables 1 and 2). Six samples were paired samples from the same terrace level. Although none of these three age pairs provided matching ages, careful scrutiny of the sample context reconciles most of the apparent discrepancies between paired samples. The remaining mismatches indicate that additional sampling and analyses are required to improve the age measurements of these geomorphic surfaces.

4.1. Kok-jar Terraces

The Kok-jar River flows south from the Moldo Range at the northern margin of the Naryn Basin to its confluence with the Naryn River near the basin outlet (Figure 1b). Strata of the underlying Chu formation are folded into a broad anticline (Figures 3a and 4a). Two prominent, broadly folded terrace levels are preserved on the westside of the Kok-jar River (Figure 3a). East of the Kok-jar River, a third terrace remnant ("eastern remnant" in Figure 3a) is preserved across the steep northern limb of the same anticline (Figure 3a).

Five kilometer long surveys of the surfaces west of the river (Figure 3a) capture the geometry of this long-wavelength fold. Assuming that the abandoned terraces had an original gradient similar to the modern river, the high and low terrace levels record a minimum of 51 m and 20 m of differential uplift, respectively (Figure 4c). Although both of these terraces are well preserved across the crest of the anticline, they do not unambiguously capture the northern hinge of the fold. As a result, uplift measurements are minimum values. The terrace remnant east of the Kok-jar Valley (Figure 3a), however, does record the northern fold hinge and indicates at least 80 m of differential uplift since abandonment (Figure 4c).

Deposits forming the upper Kok-jar terrace surface have an OSL age of 13 ± 1 ka (Karakou 100901 OSLB, Table 1). A charcoal sample from the lower terrace deposits has a calibrated radiocarbon age of 6 ± 0.1 ka (Karakou 100901, Table 2). A second OSL sample was collected below the lower terrace surface but yielded an age of 14 ± 1 ka (Karakou 100901 OSLC, Table 1), statistically equivalent to the age of the upper terrace deposits. We infer that a thick gravel unit aggraded in the Kok-jar Valley at least up to the level of the higher surface at approximately 13–14 ka. This age coincides with suite of terrace ages from the Naryn Basin and elsewhere in the Kyrgyz Tien Shan [*Thompson et al.*, 2002], and this concurrence suggests that this high surface along the Kok-jar River was formed as part of a regional terrace-forming interval. Subsequent incision and lateral planation by the Kok-jar River cut the lower, less-deformed terrace into this older fill.

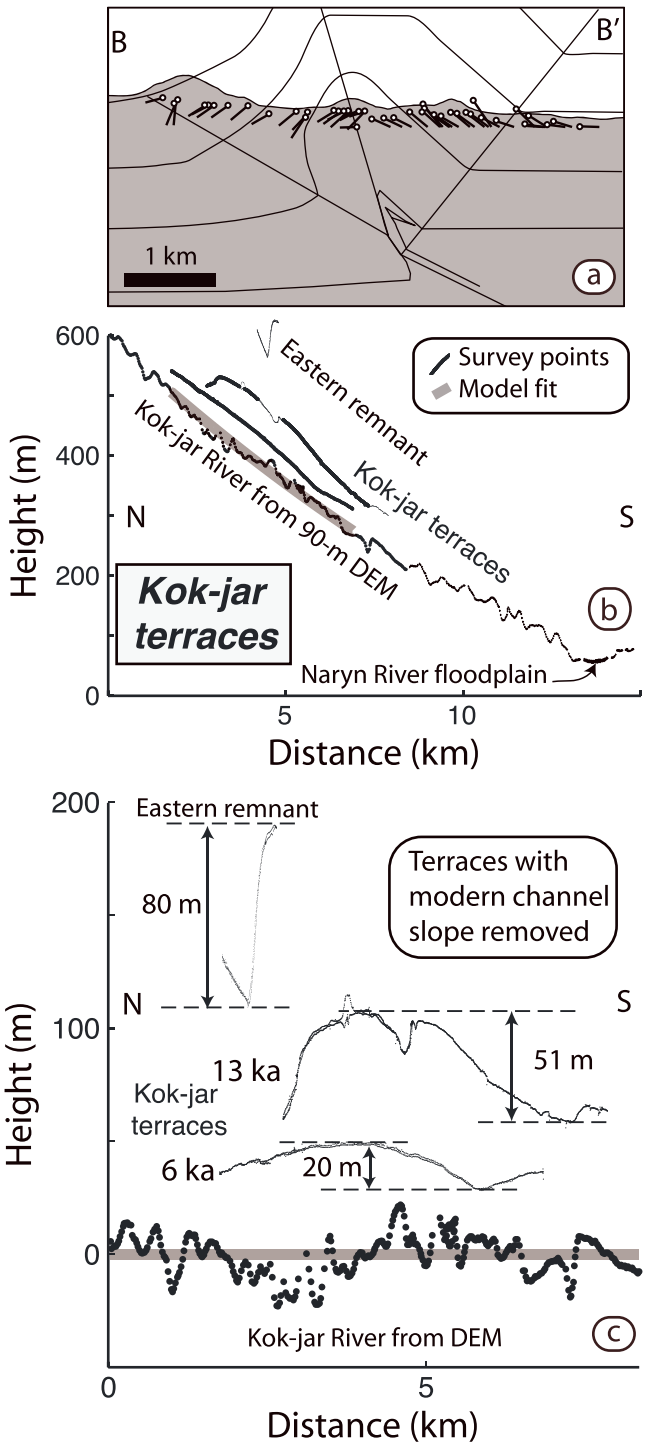

Figure 4. (a) Illustration of a north verging anticline across which the Kok-jar River has incised. (b) Terrace profiles from handheld GPS surveys mapped in Figure 3a along the Kok-jar River projected onto a line with 345° trend. Terraces record the original fluvial gradient toward the Naryn River and later folding. (c) Terrace profiles with the gradient of modern Kok-jar River removed show differential uplift recorded by each terrace level. The modern river gradient is noisy due to the limited resolution of the ASTER digital elevation model [*NASA and METI*, 2009] and the narrow canyon of the current river.

The 6 ± 0.1 ka charcoal age is interpreted to represent the time when a channel cut into the older fill and abandoned this lower surface. Based on ages of 6 and 13 ka for the lower and upper terraces, differential uplift rates are estimated as 3.3 ± 0.1 mm/yr and 3.9 ± 0.4 mm/yr, respectively.

4.2. Ak-kya Terraces

Lying 10 km to the east of the previously described Kok-jar drainage, the Ak-kya River also flows across the northern Naryn Basin from north to south from the margin of the Moldo Range to its confluence with the Naryn River (Figure 3b). Although the valley is 2–3 km wide, the river itself occupies a narrow, incised gorge. Abandoned river terraces dominate the rest of the valley floor. These terraces record progressive steepening of a north dipping fold limb. At the south end of the valley, a folded, 2.5 km long, high terrace is preserved east of the Ak-kya River (Figures 3b and 5). Two smaller inset terraces are preserved below this higher surface on the westside of the river (Figures 3b and 5). Based on constituent clast type, the ancestral Naryn River occupied the southern (north sloping) part of the highest terrace, whereas its tributary, the ancestral Ak-kya River, occupied the northern part of the same terrace (Figure 5b). As a result, the high terrace at the time of abandonment probably sloped to the south at an angle defined by the gradient of the ancestral Ak-kya River but lost this southward slope in the region where the ancestral Naryn River, flowing to the west, occupied the surface. Notably, the diffuse boundary between the paleo-Naryn surface and the Ak-kya surface lies ~3 km north of the modern Naryn River and attests to a broad floodplain prior to folding.

Differential GPS surveys of this suite of three terrace levels record the progressive deformation across a synclinal fold hinge (Figure 5b). The undeformed portion of the higher terrace gently slopes to the south-southeast at 2°. Farther south and across

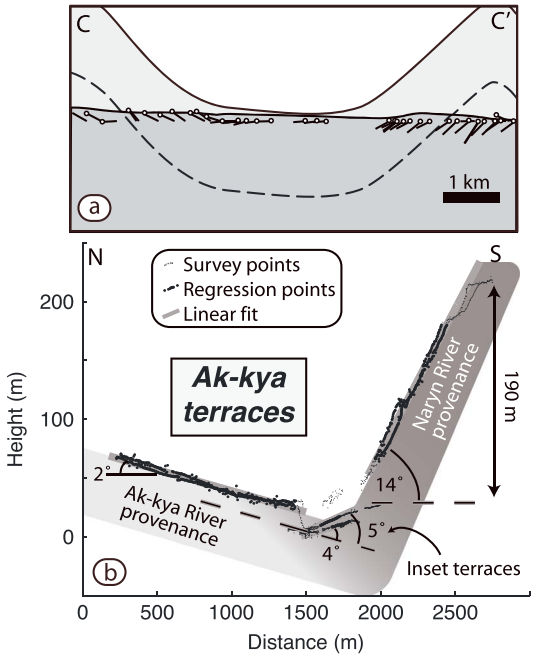

Figure 5. (a) Illustration of folded strata along the Ak-kya River (see Figure 1b for location). (b) Folded terraces from the rectangular region in part *a*. Terrace profiles from GPS surveys along the Ak-kya River are projected onto a line with 360° trend. Dashed lines represent inferred original terrace geometry. Terrace dips are calculated by linear regression through selected survey points. Note the progressive rotation of terrace dip from 4° to 5° to 14° from youngest to oldest. Data from deeply eroded terraces and major gullies were not included in the regressions.

the fold axis, the folded surface slopes toward the north-northwest at 14°. Following the standard methodology (Figure 2), this tilt suggests that since abandonment, the terrace has experienced a total of 16° of folding, but because the terrace clast composition indicates that the original terrace geometry (given its Naryn River provenance) may not have been coplanar with the upstream Ak-Kya terrace, a more conservative magnitude of folding is 14°. The crest of the fold is not preserved. Instead, the folded surface has been truncated due to headward erosion of small tributary gullies descending to the larger Naryn River to the south. The highest point of the surveyed terrace sits 190 m above the elevation that would be predicted for the ancestral Naryn River floodplain. Thus, since abandonment of the higher terrace level, the structure that the terrace transects has accommodated about 14° of rotation and more than 190 m of differential uplift.

The lower inset terraces near the fold hinge are not as broadly preserved (Figure 3b). No part of the surveys shows either the crest of the fold or a region that could confidently be described as undeformed. The upper (older) inset surface records 3° of rotation from the horizontal or 5° of rotation with respect to the broadly preserved, higher Ak-Kya terrace to its north (Figure 5b). The lower (younger) surface records 4° of rotation with respect to the same Ak-Kya terrace.

An OSL sample from the northern edge of the highest terrace along the Ak-kya River was dated at 270 ± 17 ka (S Ak-kya 100831 OSLA, Table 1). This age implies a minimum differential uplift rate of 0.7 ± 0.1 mm/yr for the northward tilted terrace. This rate is a conservative estimate because the crest of the folded terrace is not preserved.

The fold scarp preserved along the Ak-kya River records progressive steepening of terraces and bedding through time (Figure 5b). The amount of rotation recorded by each older surface increases systematically from 4° of rotation for the lowest inset surface to 14° of rotation of the highest terrace, and up to 40° recorded by the dipping Chu Formation across which the terraces are beveled.

4.3. Jaman-davan Terraces

The Jaman-davan River (Figure 1b) flows to the northwest across the southern Naryn Basin from the western terminus of the Baybeiche Range before joining the Alabuga River 9 km upstream of the Alabuga-Naryn confluence (Figure 6). Like the Ak-kya River to the northeast, the Jaman-davan River crosses a fold immediately upstream of its confluence. A single terrace level is preserved above the Jaman-davan River for more than 10 km upstream of its junction with the Alabuga River. Remarkably, this terrace level diverges into three distinct levels across the fold (Figure 7). A 9 m high erosional step, or riser, separates the lowest surface from the middle terrace level across the fold, but upstream of the fold, only a subtle riser (~1 m) disrupts the extensive terrace surface. A 34 m high riser separates the middle and highest surface across the fold, but no riser visibly separates these levels upstream of the base of the fold. The slopes and lengths of the folded terrace surfaces are summarized in Table 3.

The folded terraces (Figure 6) are formed in the footwall of a northwest dipping thrust fault that is visible in outcrop. A similarly oriented fault may underlie the folded terraces, such that the terrace deformation records

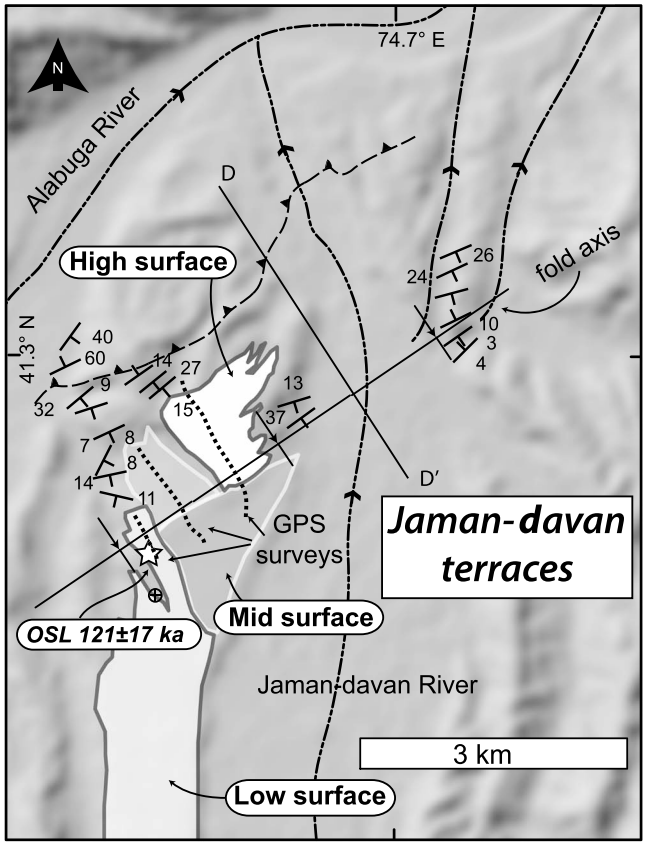

Figure 6. Three terrace levels along the Jaman-davan River (see Figure 1b for location). Terraces step down to the west, although the main river now flows along the eastern side due to subsequent river capture. The crest of the fold is truncated by a northwest dipping fault.

deformation in the forelimb above a blind thrust (Figure 7). Terrace dips lie approximately parallel to bedding. This pattern of folding by progressive limb lengthening with constant dip in the forelimb of a thrust fault is consistent with some models of fault propagation folding [*Hardy and Poblet*, 2005; *Suppe and Medwedeff*, 1990].

A sediment sample from the upstream Jaman-davan terrace yielded an OSL age of 121 ± 17 ka (Bad Pass 100905 OSLD, Table 1). This sample was collected from a silt bed 8 m below the terrace-top upstream of the toe of the fold. Because the sample site is deep below the terrace surface, we interpret the sample to have been deposited during aggradation of the fill terrace, rather than during the subsequent incision that beveled the lower two terrace levels and eventually led to complete abandonment of the surface. Even though the sample might have been deposited during formation of the one of the two lower terrace levels, such a scenario is less parsimonious. In order for the sample to closely date either of the lower two terrace levels, the river must have first incised to a depth of greater than 8 m below the terrace top before aggrading back up to the same level recorded by the terraces upstream of the fold. If the OSL sample is assumed to most closely date the highest terrace, this age implies a perpendicular offset rate of 0.7 ± 0.1 mm/yr (Table 3).

4.4. Mygachy Terraces

The Mygachy River (Figure 1b) flows northwest from the Baybeiche Range on the Naryn Basin's southern margin toward the Naryn River (Figure 8a). The river is incised below two terrace levels (Figure 9). Both terraces display deformation across a fold that trends northeast. The higher terrace is much more extensive, displays a laterally extensive fold scarp, and has a relict channel system incised into it (Figure 10). On the flank of the fold scarp, two abandoned valleys that trend along (rather than down) the fold scarp are perched above the active channel. We interpret these perched valleys and their orthogonal orientation with respect to the consequent gullies on the fold scarp as abandoned remnants of the active stream channel that were channelized parallel to the base of the fold scarp and have been subsequently advected up onto the fold scarp. These drainage features indicate that the ground surface and underlying strata have been translated through an axial surface as the geologic fold has grown.

The Mygachy terraces are deformed by an abrupt kink in their surface at the crest and toe of a fold limb (as illustrated in Figure 2). These deformed terraces and the bedding underlying them record folding above a fault bend (Figure 9). The spatial coincidence of the toe of the fold with the kink in the underlying strata argues for sustained deformation in a similar geometric shape through time, as has been described for fold scarps elsewhere [*Chen et al.*, 2007].

Along the Mygachy River (Figure 8a), two samples from the high surface yield strikingly different OSL ages of 593 ± 50 ka and 175 ± 13 ka (Akchiy 100902 OSLA and Akchiy 100902 OSLb, Table 1). Given the 87 m of perpendicular offset of this surface, i.e., the offset measured perpendicular to the unfolded terrace tread

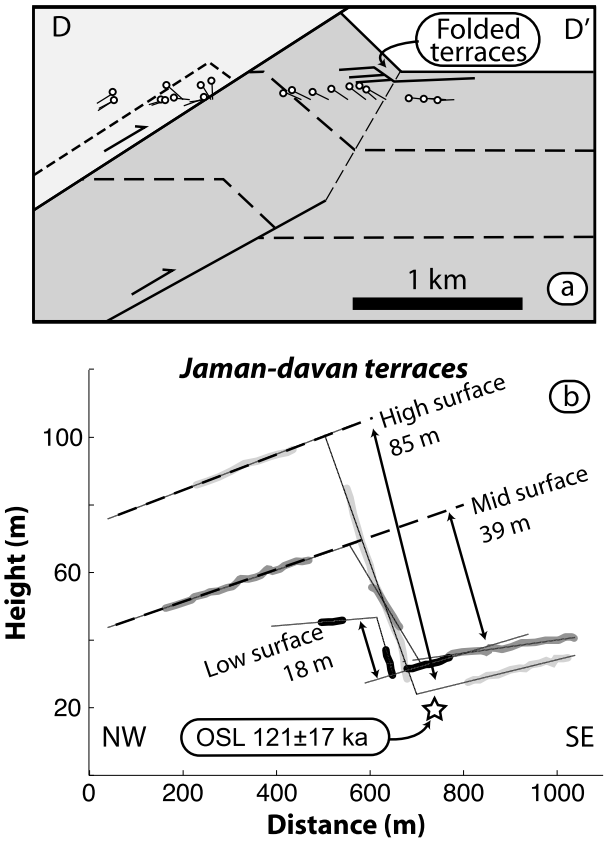

Figure 7. (a) Cross section through the fault propagation fold that has deformed terraces of the Jaman-davan River (see Figure 6 for locations). (b) Survey profiles of terraces along the Jaman-davan River. Fold offsets are measured through the midpoint of each tilted limb. Note that the middle and high surfaces merge southeast of the fold. This deformation pattern indicates progressive lengthening of the fold scarp but not progressive rotation.

(Figure 2), its mismatched old and young ages imply perpendicular offset rates of 0.15 ± 0.02 and 0.5 ± 0.04 mm/yr, respectively. Because the sample yielding the older age (and slower rate) failed the dose recovery test [*Murray and Wintle*, 2000, 2003], it is deemed less reliable, and the younger age that yields the faster rate is preferred.

Along the Mygachy River, two ages were produced for the lower terrace (Figure 9d) which is folded across the same underlying structure as the high surface. An OSL sample was collected from a 60 cm thick silt bed within a gravel conglomerate situated nearly 1 km upstream from the fold toe and yielded an age of 66 ± 9 ka (Cemetery 100905 OSLA, Table 1). From a fine-grained deposit lying atop the cobble-dominated terrace, a charcoal sample yielded an age of 44 ± 1 ka (Cemetery 100905, Table 2). This younger age from deposits stratigraphically above the OSL sample demonstrate the reasonableness (but not correctness) of the OSL age. Because this fine-grained deposit modifies the upstream slope of the surveyed terrace top and lies immediately upstream of the fold scarp (Figure 9d), this prism of younger sediment is interpreted as having

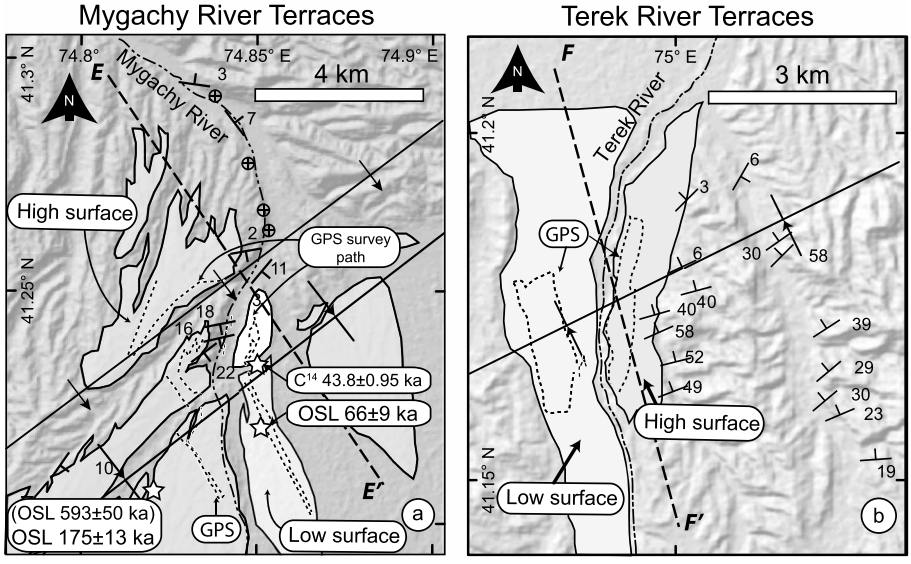

Figure 8. (a) Folded fluvial terraces in the vicinity of the Mygachy River (see Figure 1b for location). Dashed paths on terrace surfaces show locations of differential GPS surveys (Figure 9). White stars show OSL and charcoal sample locations. (b) Two terrace levels preserved above the Terek River near the southern basin margin (see Figure 1b for location).

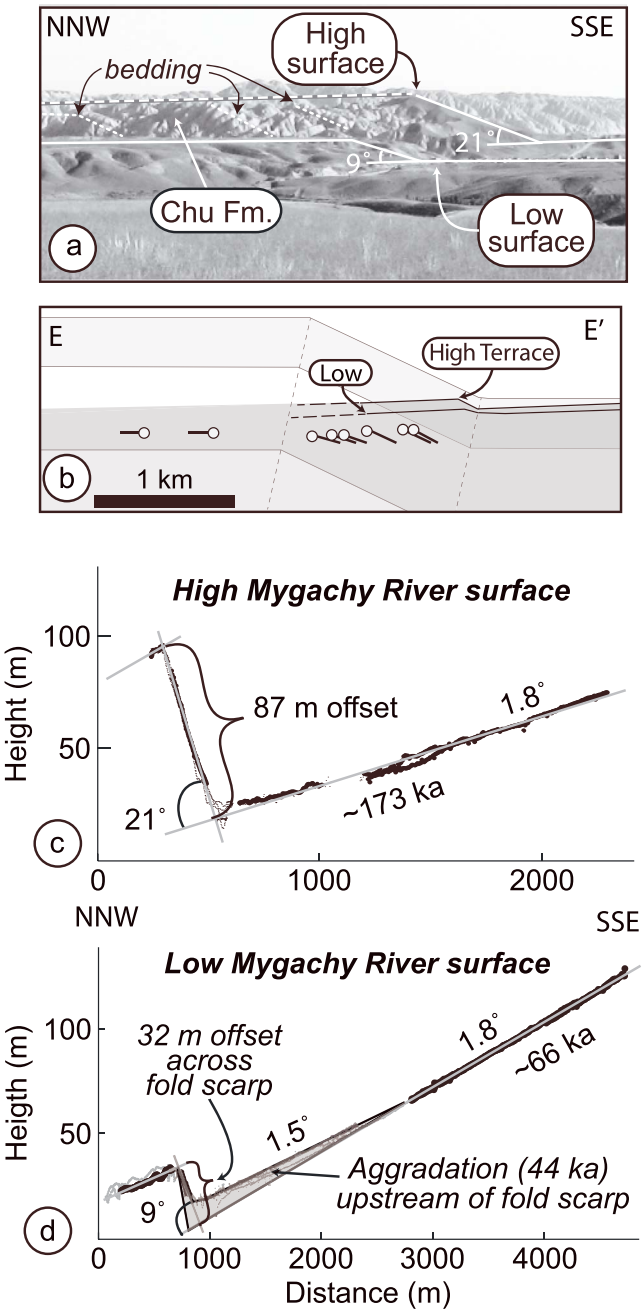

Figure 9. (a) Photograph looking to the NE and depicting two folded terraces preserved along the Mygachy River. (b) Illustration of deformed terrace and folded strata underlying the terrace along the Mygachy River. (c) GPS survey points from the high terraces of the Mygachy River. (d) The low terrace surface has experienced aggradation upstream of the fold that reduces its surface gradient. Survey points are projected onto a line with a trend of 320° (approximately perpendicular to the fold axes).

accumulated due to sediment ponding immediately upstream of the growing fold scarp. Thus, this portion of the survey data is not used to calculate terrace offset, and its age is regarded as a minimum limiting age for the terrace surface on which it sits.

The perpendicular offset rate calculated from the OSL age and the unmodified terrace gradient upstream from the fold toe on the lower Mygachy River terrace is 0.5 ± 0.1 mm/yr, which is statistically equivalent to the perpendicular offset rate calculated from the more reliable OSL age (the younger of the two ages) for the higher Mygachy River terrace (Table 3). These data imply that rate of vertical deformation has remained nearly constant at ~0.5 mm/yr for the past 175 ka.

4.5. Terek River Terraces

The Terek River flows to the north out of the Baybeiche Range on the southern margin of the Naryn Basin (Figure 8b). The regional unconformity separating bedrock from Cenozoic strata defines the southern flank of the Baybeiche Range, where the overlying strata have been stripped away. To the north of the exposed bedrock and toward the center of the Naryn Basin, Cenozoic strata dip parallel to the unconformity. Bedding maintains a ~30° dip to the north of the exposed unconformity surface until dips become abruptly gentler at a synclinal kink marking the northern limit of the fold associated with uplift of the Baybeiche Range. This mountain range-scale fold is almost certainly related to a north dipping fault system that daylights more than 10 km to the south in the At-Bashi Basin (Figure 1a).

Multiple deformed fluvial terraces that traverse the kink are carved into tilted bedding on the backlimb of the Baybeiche Range (Figure 8b). Only two of these terraces are broadly preserved. The terraces are folded along the same axial trace that is defined by the underlying Cenozoic bedding.

Terraces above and below the Terek River fold scarp (Figure 11) have gentle dips that are similar to the modern river gradient. The higher fold scarp is steeper than the lower fold scarp but neither is as steep as the underlying bedding. The toe of the fold scarp corresponds to a kink in the underlying Chu Formation, but

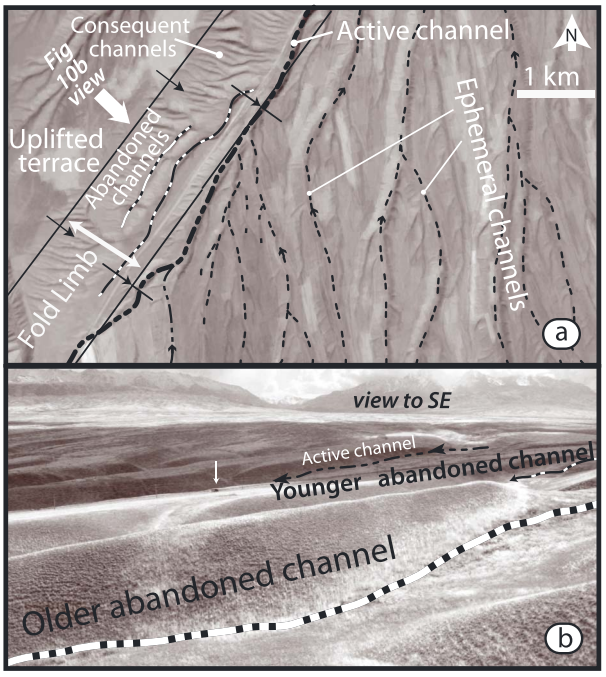

Figure 10. (a) Map view of channel patterns incised the high terrace surface south of the Mygachy River. The active channel, a tributary of the Mygachy River, flows parallel to the fold scarp. Ravines cut by the channel have been sequentially abandoned during lateral advection of the surface up the fold scarp. Satellite image is from *Google Earth*. (b) Photograph toward the SSE looking down the fold scarp into abandoned channel scars. Small white arrow indicates an automobile for scale.

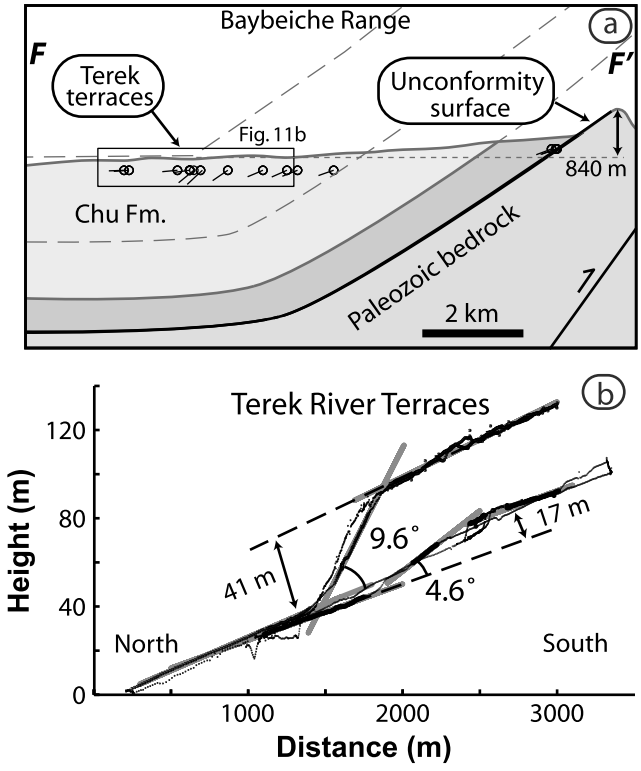

Figure 11. (a) Simplified cross section across the northern flank of the Baybeiche Range showing Cenozoic Basin sediment overlying folded unconformity surface in the vicinity of the Terek River. (b) GPS surveys from the vicinity of the Terek River in profile view trending 180° (Figure 8b).

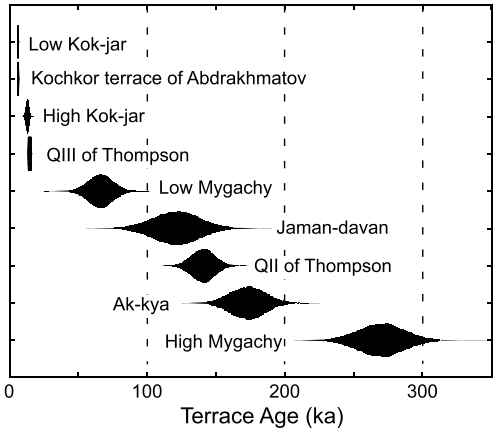

Figure 12. Comparison between terrace ages across the western Naryn Basin (this study) and regional terrace surfaces (QII-QIV) [*Abdrakhmatov et al*., 2001; *Thompson et al*., 2002]. The probability distribution associated with each age is represented by the varying width of each marker.

the crest of the fold scarp does not coincide with a change in the underlying bedding. This geometry indicates a similar deformation pathway to that found along the Mygachy River (Figure 8a), whereby the fold scarp grows in height as material is advected through the axial surface at the toe of the fold [*Chen et al*., 2007].

Because no suitable material for age determination was found in the deposits of either terrace level, we estimate the age of the Terek terraces based on correlation to nearby geochronologic control. Other work in the region suggests a vertical exhumation rate of the northern flank of the Baybeiche Range of ~0.7–2 mm/yr [*Oskin et al*., 2014]. Additionally, we make a speculative temporal correlation of the high and low Terek terraces with the middle and lowest Jaman-davan river terraces. Similar to the Terek River, the Jaman-davan River issues from the Baybeiche Range and displays prominent terrace levels that merge into a single level where they are not deformed by an underlying structure (Figure 10). The 0.7 ± 0.1 mm/yr offset rate from the high Jaman-davan terrace implies that the low- and mid-Javan-davan terraces may have ages of 55 ± 8 ka and 25 ± 3 ka, if deformation rates remained steady, as suggested by other nearby structures. Given the uncertainties associated with these age estimates, the ~55 ka age estimate of the middle surface is statistically equivalent to the 66 ± 9 ka age of the lower terrace preserved along the nearby Mygachy River. This tentative correlation of the Jaman-davan terraces to the Terek terraces implies perpendicular offset rates of 0.8 ± 0.1 and 0.7 ± 0.1 mm/yr across the high and low Terek terraces. Though speculative, this rate is consistent with the millennial exhumation rate calculated by *Oskin et al*. [2014] using cosmogenic nuclides.

4.6. Naryn Lake Terraces

One charcoal sample was collected from light-colored silts that fill a narrow, side-valley draining to the Naryn River. We interpret these sediments as having been deposited near the top of the lacustrine sequence of the landslide-dammed "Naryn Lake" [*Korup et al*., 2006]. As such, this sample's calibrated age of 1430 ± 55 years B.P. represents the first absolute age constraint on this sedimentary unit and the causative landslide. Given this young age, it is not surprising that the lacustrine fill surface was not visibly deformed across any geologic structures.

5. Discussion

5.1. Regionally Recognized Terraces

Previous dating of deformed terrace surfaces across the Kyrgyz Tien Shan, including the Naryn Basin, suggested that most broadly preserved terrace levels had ages representing two temporally discrete periods of climatically related, regional terrace formation [*Thompson et al*., 2002]. These regional Quaternary terrace levels are often assigned Roman numeral labels in Russian and English publications. The older QII terrace apparently formed during the penultimate deglaciation 135–125 ka and the younger QIII terrace formed during the last glacial-interglacial transition 14–10 ka [*Fairbanks*, 1989; *Imbrie*, 1984; *Shackleton*, 2000]. As presented here, the new suite of dated terrace levels from the interior of the Tien Shan includes some dates that appear to match these climatic perturbations (Figure 12). In particular, the high Kok-jar terrace and the Jaman-davan terrace may have been formed during the last and the penultimate deglaciations, respectively. Many of our new dates, however, fall outside of these two regionally recognized terrace levels. The younger, 6 ka, surface along the Kok-jar River has not been dated elsewhere in the Naryn Basin, but it may, nonetheless, be related to a regional terrace-forming event because a terrace of equivalent age was dated along the Djaunarik River in the Kochkor Basin, 120 km to the northeast [*Abdrakhmatov et al*., 2001].

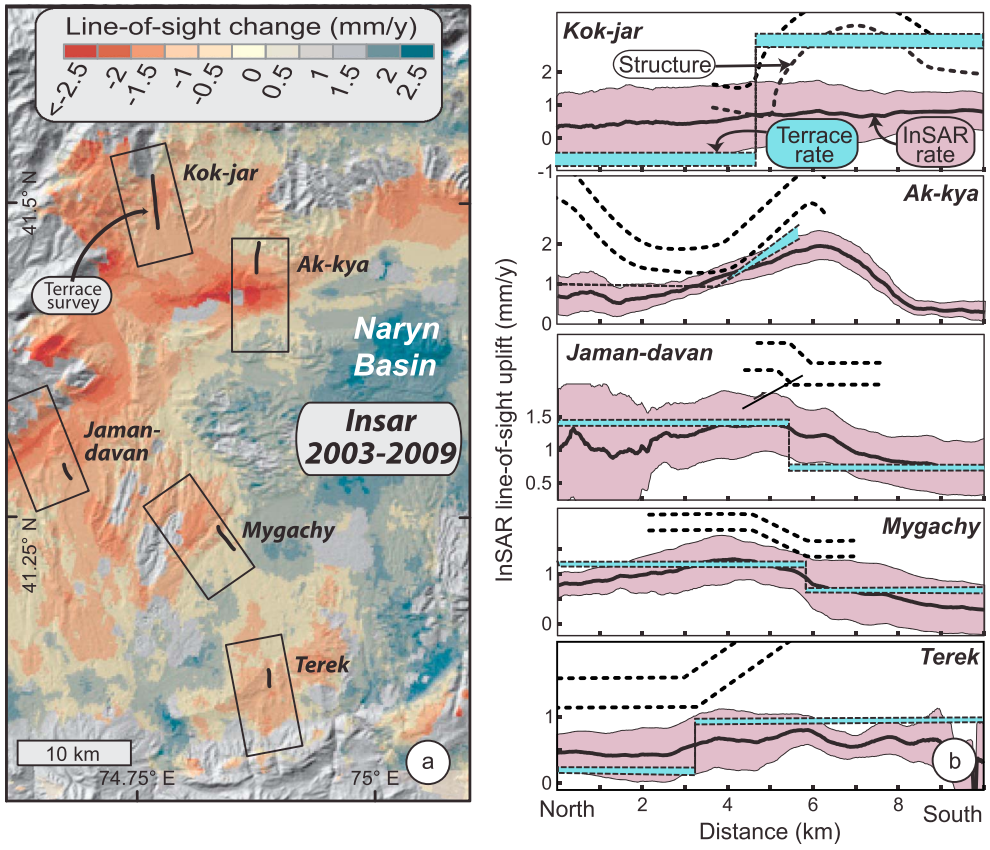

Figure 13. (a) InSAR map of line-of-sight surface deformation rates [*Goode et al*., 2011]. Negative values (red) show motion toward the satellite. Boxes depict mapped examples from this study with survey lines shown. (b) Comparison among InSAR deformation rates, geologic deformation rates, and geologic structures at each of five study sites across the western Naryn Basin. Mean InSAR rate (black curve) and standard error from weighted variance (pink region) are shown from data within a 5 km wide swath. The calculated perpendicular offset rates across each structure are illustrated as steps with the uncertainty in step height shown in blue. Note that InSAR measurements cover a large spatial area, but geologic rates apply more narrowly to a particular structure. Form lines of underlying strata (black dashed curves) show structural geometry without vertical exaggeration. Except for the Kok-jar section, InSAR rates and the geologic rates roughly match each other at each locality.

We also sampled older terrace levels that yielded ages of 175 and 270 ka. These older terrace levels may have formed during earlier perturbations to central Asian climate [*Karabanov et al*., 1998; *Peck et al*., 1994]. Alternatively, dating of additional high terrace levels in the Tien Shan may indicate that they are of only local significance. The broad preservation of these older terrace levels suggests, however, that simply assuming that any high, deformed terrace level in the Tien Shan formed during the penultimate deglaciation may underestimate its true age and would cause deformation rates that are associated with such surfaces to be unrealistically rapid [*Hetzel et al*., 2002].

5.2. Quaternary Rates Compared to InSAR

The deformation rates calculated at the five study sites across the western Naryn Basin represent the rates of folding averaged over tens of thousands of years. We compare these rates, which span many earthquake cycles, to geodetic measurements from InSAR, which span only 6 years [*Goode et al*., 2011]. InSAR rates from the western Naryn Basin (Figure 13a) show the rates of ground surface motion toward the satellite relative to the average rate across the image. At each of the five study localities, we measure mean InSAR rates across a 5 km wide swath oriented perpendicular to the underlying structure (Figure 13b). Average annual line-of-sight range change is calculated along the swaths in each of five interferograms that form the average line-of-sight rate map (Figure 13a). Uncertainty bounds represent the standard error of the average annual range change weighted by the time span of each interferogram. In most cases, a zone of line-of-sight relative uplift recorded

in the InSAR data corresponds with the underlying geologic fold reconstructed from bedding attitudes (Figure 13b). Moreover, many of the perpendicular offset rates measured from deformed terraces at millennial or greater timescale are consistent with the short-term InSAR rates.

Because the geodetic uncertainties are large, we cannot reject the possibility that the interseismic rates measured by InSAR and geologic rates from terrace measurements differ by as much as 50% across some structures. Even though neither InSAR nor the terrace offset measurements record only vertical displacement, they each closely approximate it. Given the typical orientation of structures in the Naryn Basin and the satellite acquisition geometry, numerical models show that InSAR measurements of deformation rates are a close approximation of vertical uplift rates [*Goode et al*., 2011]. The component of terrace deformation recorded with GPS surveys is measured perpendicular to undeformed surfaces that commonly dip at 2° and, hence, is also close to vertical.

Although the geologic and geodetic patterns match remarkably well across Naryn Basin structures, such a close correspondence between the two is not generally expected [*Allmendinger et al*., 2009]. A multitude of interseismic and even nontectonic deformation patterns may cause short-term deformation patterns to differ from the long-term pattern recorded in outcrops. During the interval between earthquakes, deformation may be distributed across tens of kilometers surrounding a locked fault, rather than being focused on individual geologic structures [e.g., *Wright et al*., 2004]. Where interseismic surface deformation is observed to coincide with active structures, this deformation is commonly attributed to shallow creep along faults [e.g. *Huang et al*., 2006]. Because four of five study sites with adequate InSAR coverage all show agreement between geologic and InSAR deformation rates, we infer that the modern deformation pattern results from shallow fault creep. The exception to this pattern of shallow fault creep in the Kok-jar structure where the InSAR rate is so much lower than the geologically defined rate that uncertainty bounds on the rates do not overlap. Based on this discrepancy between long-term and short-term rates, this fault underlying the Kok-jar fold may be locked, resulting in a diminished interseismic deformation signal.

Along the Mygachy and Kok-jar Rivers where multiple terrace levels have been dated across the same structure, the rates calculated based on the offset of each surface are internally consistent. Such consistency implies a nearly constant rate of folding that has prevailed for millennia. The agreement between the geologic rates and modern geodetic rates further supports the inference that average deformation rates across several structures have remained rather steady over many millennia.

Several caveats are relevant to the apparent concurrence of long- and short-term rates. The geologic rates across the Jaman-davan terraces are uncertain not only because of analytic uncertainty in the sample age (121 ± 17 ka) but also because it is unclear which of the three deformed terraces levels this sample most closely dates. Similarly, the rates calculated from Terek River terraces are speculative, because they are based only on correlation to terrace levels in the Jaman-davan River. Although these estimated rates are based on geologic rationales, they are consistent with the InSAR rates that support these otherwise tentative rate calculations.

5.3. Initiation Ages of Naryn Basin Structures

The suite of terrace surveys described here (Figures 3 through 11) traverses each of the major folds along a transection of the western Naryn Basin. To derive a rough estimate of the age for the initiation of each structure across the basin, we use a Monte Carlo simulation to combine (i) the total deformation accumulated since initiation of the structure with (ii) a steady long-term rate of deformation derived from the deformed terraces (Figure 14). On most of the structures across which terraces have been deformed, we are able to constrain total deformation that has affected the underlying Cenozoic strata. Because the crest of the fold along the Jaman-davan River is truncated by a fault with unknown offset (Figure 7), we do not estimate the total deformation across this structure.

The most northern structure within the western Naryn Basin (Figure 1b) is the broad anticline traversed by the Kok-jar River. Both the high and low Kok-jar River surfaces indicate differential uplift rates of ~3.5 mm/yr (Figures 3 and 4). Reconstruction of the shape of the folded strata in the anticline implies 1.1 ± 0.2 km of relative uplift (Figure 4). Because the hinge zone recorded in the strata is broad, we assign a 20% uncertainty to this measurement. To estimate the initiation of the Kok-jar anticline, we pool the uplift rates calculated from the two terrace levels and assume uniform deformation rates through time. With these assumptions, the Kok-jar anticline is estimated to have initiated at 0.3 ± 0.07 Ma (Figure 14).

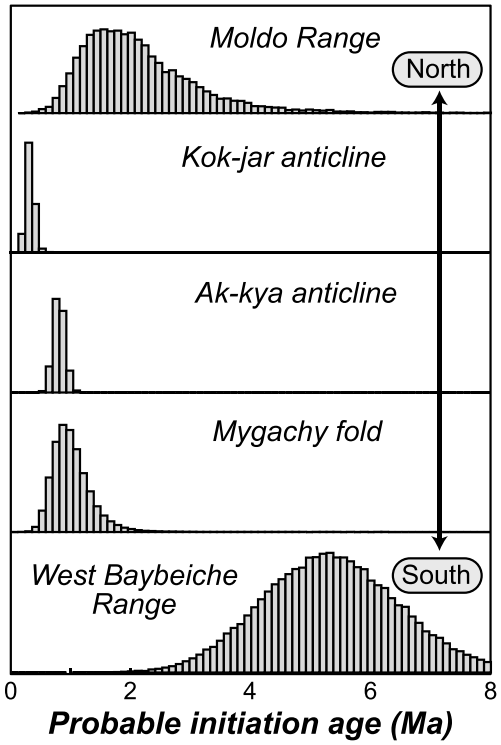

Figure 14. Probable ranges of initiation ages for structures in the western Naryn Basin. All ages are based on the assumption that deformation rates have remained constant throughout the growth of each structure. Probability distributions result from Monte Carlo simulation of uncertainties in both deformation rates and total deformation across each structure.

Across the next structure to the south, which is cut by the Ak-kya River terraces (Figures 3 and 5), comparison of deformed terraces to the underlying bedding orientation constrains the deformation pathway of the Ak-kya anticline. The inset terraces, the high terrace, and the dip of underlying strata indicate progressive rotation of the north limb of the anticline (Figure 5). Assuming that the rate of limb rotation has been constant through time, we can estimate the onset of deformation. The 14° slope of the 270 ka Ak-kya terrace surface indicates a rotation rate of $5.1 \pm 0.3 \cdot 10^{-5}$°/yr. The underlying strata have a dip of 40 ± 4° (we assign a 10% uncertainty to the structural measurements) suggesting an initiation age of 0.8 ± 0.1 Ma (Figure 14).

Farther south along the Mygachy River (Figures 8–10), we find abundant evidence that the deformed terraces and underlying strata are advected through the axial surface at the toe of the fold through time. The perpendicular offset measured between the crest and toe of a folded marker (terrace or stratum) can be used to quantify the magnitude of displacement across the structure [*Chen et al*., 2007; *Suppe et al*., 1992; *Thompson et al*., 2002]. The rate of offset that is calculated from the high and low Mygachy River terraces is ~0.5 mm/yr. Reconstructing the location of the upper and lower kinks preserved in the underlying strata indicates a total offset of about 610 ± 120 m. Assuming that the offset rates estimated for the last 175 kyr have prevailed since the structure initiated, the Mygachy structure began to develop at 1.0 ± 0.3 Ma (Figure 14).

The unconformity surface preserved on the northern flank of the Baybeiche Range and below Cenozoic Basin-filling strata records the total offset across the range [*Burbank et al*., 1999]. A stratigraphic section measured along the Terek River indicates that 3 km of strata overlie the unconformity surface at this location (Figure 11a) [*Omuraliev*, 1978]. Erosion of the resistant rocks forming the range crest has likely been minor because the topographic crest of the Baybeiche Range defines a fairly smooth, bow-shaped profile reminiscent of its tectonic origins, not later modification by deep erosion [*Burbank et al*., 1999]. The range crest above the Terek River Valley sits 840 m above the Terek River terraces. Again, we assign a 20% uncertainty to the measurement, which yields 3.8 ± 0.8 km of relative vertical displacement across the Baybeiche Range structure. Exhumation rate estimates of the Baybeiche Range [*Oskin et al*., 2014] and tentative correlation of the Terek terraces with the Jaman-davan terraces suggest an uplift rate of roughly 0.6–0.9 mm/yr.

An assumption of a constant deformation rate implies initiation of the Baybeiche Range structure before 5.3 ± 1.2 Ma. This locality near the western terminus of the Baybeiche Range may have begun to deform later or have been offset at a different rate than the higher central part of the range, such that this age may not apply to the initiation of the entire, potentially segmented, range [*Burbank et al*., 1999].

In a previous study of deformed terraces ~100 km east of these study sites in the central Naryn Basin, *Thompson et al*. [2002] calculated Late Quaternary horizontal shortening at a rate of 4.2 ± 0.7 mm/yr across the Moldo Range, which marks the northern margin of the Naryn Basin. Even though these measurements were made on faults within the basin interior, the structures appeared to accommodate shortening associated with uplift of the Moldo Range. In order to estimate the total shortening across the Moldo Range

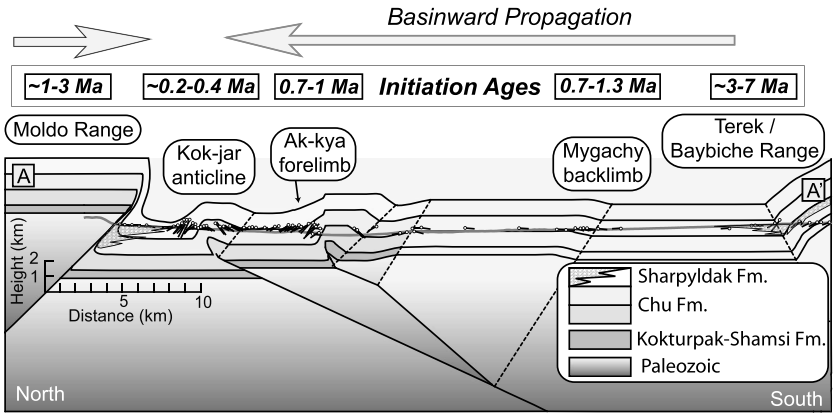

Figure 15. Balanced cross section across the western Naryn Basin modified after *Goode et al*. [2011] (see Figure 1b for location). Deformation of fluvial terraces at three different study sites may be related to slip on a single south dipping thrust system.

at the northern Naryn Basin margin, we use published estimates of range-bounding fault dip and deflection of the unconformity surface across the northern basin margin. Maps of the topography of the unconformity that underlies the Cenozoic strata show ~8 km of relief between the highest remnants of the unconformity in the Moldo Range and the deepest portion of the Cenozoic Basin fill near the northern edge of the basin [*Abdrakhmatov et al*., 2001; *Cobbold et al*., 1996; *Omuraliev*, 1978, 1988]. Based on outcrop observations, aftershock clustering [*Ghose et al*., 1997], earthquake focal mechanisms [*Molnar and Ghose*, 2000], and a magnetotelluric study [*Park et al*., 2003], relatively steep reverse faults dipping at ~45° are commonly associated with major Kyrgyz earthquakes and uplift of basin-bounding ranges. We assign a 10% uncertainty both to the 8 km vertical offset of the unconformity that underlies Cenozoic strata and to the inferred 45° dip of the causative fault. Extrapolation of the Quaternary shortening rate into the past indicates that this shortening could have accumulated since 2 ± 1 Ma (Figure 14). Of the five estimated initiation ages, this estimate for the Moldo Range is probably the most uncertain and may represent only a lower limit. Estimating total shortening from the vertical offset of an unconformity is difficult because the dip of the causative fault is unknown, the unconformity is commonly poorly preserved at the Moldo Range crest, and the thickness of sediment overlying the erosion surface near the range front is uncertain. Finally, the shortening rate calculated for the Moldo Range 90 km to the east in the central Naryn Basin might not be representative of the Moldo Range in the western Naryn Basin where shortening may be accommodated across a greater number of structures.

The structures in the interior of the Naryn Basin that deform the Kok-jar, Ak-kya, and Mygachy River terraces have all initiated since ~1 Ma (Figure 14). The probable onset ages of the Ak-kya and Mygachy folds overlap so that we cannot reject the possibility that deformation commenced simultaneously across these two structures. The Kok-jar fold likely initiated somewhat more recently. A balanced cross section through the western Naryn Basin [*Goode et al*., 2011] shows these three structures to be related to the same south dipping fault system: a geometry consistent to apparent synchrony of basin-interior deformation (Figure 15). Although this area-balanced cross section does not transect the Jaman-davan structure, the cross section does provide a context for the other four study sites. In this structural interpretation, the broadly warped terraces along the Kok-jar River (Figure 4) record slip on a blind, south dipping thrust. This thrust merges at depth with a second, south dipping fault. Propagation of this second thrust fault toward the surface has caused progressive rotation and steepening of the Ak-kya River terraces (Figure 5) in the forelimb of a fault-related fold. Farther south, the southeast dipping terraces along the Mygachy River (Figure 9) record deformation related to the junction of these two south dipping faults at depth. In this interpretation, a fault-bend fold has formed as a result of the change in the dip above the same south dipping fault responsible for steepening of the Ak-kya terraces. Finally, the deformation of terraces along the Terek River records the uplift of the pre-Cenozoic unconformity and overlying strata in the Baybeiche Range (Figure 11).

These new estimates for the onset and migration of deformation in the Naryn Basin provide some insights on the tectonic evolution of the broader Tien Shan. The temporal-spatial pattern of deformation indicates a

multistage disruption of a large, late Miocene Basin spanning much of the region between the newly emergent Kyrgyz Range in the north [*Bullen et al.*, 2001, 2003] and ranges associated with the Maidan thrust in the south [*Sobel et al.*, 2006a] (Figure 1a). The presence of this contiguous basin is supported both by its regionally correlative Eocene-Miocene stratigraphy [*Abdrakhmatov et al.*, 2001] and by the thermochronologically recorded burial reheating of Paleozoic and Mesozoic bedrock that later emerged as Plio-Pleistocene ranges in the northern Tien Shan [*Glorie et al.*, 2010]. Our conclusion that the ranges currently bounding the Naryn Basin began to grow during Plio-Pleistocene times eliminates the possibility of a single wave of deformation migrating across the nascent Tien Shan between 24 and 10 Ma. Nor do the data allow for a steady propagation rate of deformation across the orogen, because both the Moldo and Baybeiche Ranges lie in the middle of the Tien Shan (Figure 1), yet record initial deformation as young as 1–3 Ma (Figure 14). Together with the late Miocene-Pleistocene emergence of several other ranges within the Kyrgyz Tien Shan [*Glorie et al.*, 2010; *Macaulay et al.*, 2013], our data indicate that significant out-of-sequence thrusting characterized the growth of the Kyrgyz Tien Shan. In contrast, at the basin scale, our newly dated structures (Figure 14) indicate encroachment of in-sequence deformation across the Naryn Basin during the past 1.5 Myr. Finally, the balanced cross section [*Goode et al.*, 2011] suggests that the deformation is linked to deep-seated thrust faults that dip rather steeply through the 15 to 20 km thick, brittle crust, similar to the fault that failed during the nearby M_s 7.3 1992 Suusamyr earthquake [*Ghose et al.*, 1997]. Reverse faulting in both Naryn and Suusamyr Basins may be influenced by inherited normal [*Sibson and Xie*, 1998] or strike-slip [*Macaulay et al.*, 2013] faults of Paleozoic or Mesozoic age. Accumulated slip on these faults is only a few kilometers and suggests that even if they follow relict structural trends, they are newly formed as late Cenozoic structures.

Although as much geodetic shortening (~20 mm/yr) is currently being absorbed across the western Tien Shan as is accommodated across the Himalaya [*Meade*, 2007; *Zubovich et al.*, 2010], the magnitude of crustal shortening is about an order of magnitude less across the Tien Shan (35–80 km versus >700 km) [*Abdrakhmatov et al.*, 2001; *Robinson*, 2001]. Only about half of this difference can be accounted for by the 25 Myr age difference in the onset of deformation between these ranges. Instead, the style of deformation has been profoundly different. In the Himalaya, the stacking of Cenozoic thrust sheets and large displacements on relatively low-angle faults (with or without channel flow) have accommodated hundreds of kilometers of shortening [*Hodges*, 2000; *Robinson*, 2001]. In contrast, the Tien Shan comprises discrete ranges that are separated by 15 to 50 km wide intramontane basins and that commonly preserve remnants of the early Cenozoic regional unconformity along their flanks. Given the interpretation that these ranges are also bounded by steeply dipping, deep-seated faults, the dominance of Paleogene or older cooling ages [*Glorie et al.*, 2010; *Macaulay et al.*, 2013] dictates that only modest Cenozoic slip has accumulated on these faults. The disruption of the Quaternary Naryn and Suusamyr Basins suggests that continued Tien Shan shortening is being accommodated, at least in part, by newly active, steep, deep-seated faults. Over time, such deformation could be expected to cannibalize the intermontane basins and produce a more continuous series of closely spaced ranges spanning the Tien Shan orogen.

6. Conclusions

Deformation rates calculated from dated, deformed surfaces in the Naryn Basin of central Kyrgyzstan are generally consistent with modern geodetic measures of rock uplift using InSAR across the same structures. Thus, each of the folds found to deform Quaternary river terraces also continues to deform the modern ground surface and persists at apparently similar rates. Based on these rates, mapping of the underlying structures, and assumed steady deformation through time, the interior of the Naryn Basin commenced to be deformed by a series of thrust faults within the last 1 My. In contrast, the Moldo and Baybeiche Ranges, both bedrock ranges that bound the basin to its north and south, respectively, began to grow at least 1–4 Myr earlier.

These estimates for the onset of deformation in and around the Naryn Basin are young compared to the 10–11 Ma estimates for the exhumation of other ranges in the Kyrgyz Tien Shan that lie to the north or the >20 Ma ages estimated for the ranges along the southern margin of the Tien Shan in China. Thus, the central Tien Shan did not grow sequentially or steadily from south to north. Instead, deformation of the orogen's interior began long after the marginal ranges had been established. As seen in recent Kyrgyz earthquakes, this out-of-sequence deformation appears to be driven by slip on steep, perhaps nascent reverse faults that

penetrate through the brittle crust. Persistence of this mode of deformation will gradually replace the current intramontane basins with bedrock-cored ranges.

Acknowledgments
Major funding for this work was provided by the National Geographic Society, Committee for Research and Exploration (8685–09). We gratefully acknowledge NASA (NNX08AG05G) and the National Science Foundation (EAR 0819874) for providing additional support. We wish to acknowledge the European Space Agency (ESA) for providing raw InSAR data at reduced cost. Mirlan Daiyrov gave us invaluable assistance in Kyrgyzstan. We thank Kanatbek Abdrakhmatov for help with logistics and Phil Toms for expedited OSL dating. Early discussions in the field with Mike Oskin and Jacob Selander motivated this contribution. Incisive reviews by M. Oskin and an anonymous reviewer greatly improved this submission. Geochronology data may be downloaded from http://www.geol.ucsb.edu/faculty/burbank/Site/Publications.html.

References

Abdrakhmatov, K. Y., et al. (1996), Relatively recent construction of the Tien Shan inferred from GPS measurements of present-day crustal deformation rates, *Nature*, *384*, 450–453.

Abdrakhmatov, K. Y., R. Weldon, S. C. Thompson, D. W. Burbank, C. Rubin, M. Miller, and P. Molnar (2001), Origin, direction, and rate of modern compression in the central Tien Shan, Kyrgyzstan, *Geologiya I Geofizika* [in Russian], *Geol. Geophys.*, *42*, 1585–1609.

Allmendinger, R. W., J. P. Loveless, M. E. Pritchard, and B. Meade (2009), From decades to epochs: Spanning the gap between geodesy and structural geology of active mountain belts, *J. Struct. Geol.*, *31*(11), 1409–1422, doi:10.1016/j.jsg.2009.08.008.

Bullen, M. E., D. W. Burbank, J. I. Garver, and K. Y. Abdrakmatov (2001), Late Cenozoic tectonic evolution of the northwestern Tien Shan: New age estimates for the initiation of mountain building, *Geol. Soc. Am. Bull.*, *113*(12), 1544–1559.

Bullen, M. E., D. W. Burbank, and J. I. Garver (2003), Building the northern Tien Shan: Integrated thermal, structural, and topographic constraints, *J. Geol.*, *111*, 149–165.

Burbank, D. W., J. K. McLean, M. E. Bullen, K. Y. Abdrakmatov, and M. G. Miller (1999), Partitioning of intermontane basins by thrust-related folding, Tien Shan, Kyrgyzstan, *Basin Res.*, *11*, 75–92.

Burgmann, R., P. A. Rosen, and E. J. Fielding (2000), Synthetic aperture radar interferometry to measure Earth's surface topography and its deformation, *Ann. Rev. Earth Planet. Sci.*, *28*, 169–209.

Burtman, V. S. (1975), Structural geology of the Variscan Tien Shan, *Amer. J. Sci.*, *280*, 725–744.

Chediya, O. K. (1986), *Morphostructure and Neo-Tectonics of the Tien Shan*, pp. 313, Academia Nauk Kyrgyz CCP, Frunze.

Chen, Y.-G., K.-Y. Lai, Y.-H. Lee, J. Suppe, W.-S. Chen, Y.-N. N. Lin, Y. Wang, J.-H. Hung, and Y.-T. Kuo (2007), Coseismic fold scarps and their kinematic behavior in the 1999 Chi-Chi earthquake Taiwan, *J. Geophys. Res.*, *112*, B03S02, doi:10.1029/2006JB004388.

Cobbold, P. R., E. Sadybaksov, and J. C. Thomas (1996), Cenozoic transpression and basin development, Kyrgyz Tienshan, Central Asia, in *Geodynamic Evolution of Sedimentary Basins*, edited by F. Roure et al., pp. 181–202, Editions Technip, Paris.

Duller, G. A. T. (1996), Recent developments in luminescence dating of Quaternary sediments, *Prog. Phys. Geogr.*, *20*(2), 127–145.

Dumitru, T. A., D. Zhou, E. Z. Chang, S. A. Graham, M. S. Hendrix, E. R. Sobel, and A. R. Carroll (2001), Uplift, exhumation, and deformation in the Chinese Tian Shan, *Geol. Soc. Am. Mem.*, *194*, 71–100.

Fairbanks, R. G. (1989), A 17,000-year glacio-eustatic sea level record: Influence of glacial melting rates on the Younger Dryas event and deep-ocean circulation, *Nature*, *342*(7), 637–642.

Galbraith, R. F. (1990), The radial plot: Graphical assessment of spread in ages, *Int. J. Radiat. Appl. Instrum. Nucl. Tracks Radiat. Meas.*, *17*(3), 207–214.

Ghose, S., M. W. Hamburger, and J. Virieux (1998), Three-dimensional velocity structure and earthquake locations beneath the northern Tien Shan of Kyrgyzstan, central Asia, *J. Geophys. Res.*, *103*, 2725–2748.

Ghose, S., R. J. Mellors, A. M. Korjenkov, M. W. Hamburger, T. L. Pavlis, G. L. Pavlis, M. Omuraliev, E. Mamyrov, and A. R. Muraliev (1997), The Ms = 7.3 1992 Suusamyr, Kyrgyzstan, earthquake in the Tien Shan; 2, Aftershock focal mechanisms and surface deformation, *Bull. Seismol. Soc. Am.*, *87*(1), 23–38.

Glorie, S., J. De Grave, M. M. Buslov, M. A. Elburg, D. F. Stockli, A. Gerdes, and P. Van den haute (2010), Multi-method chronometric constraints on the evolution of the Northern Kyrgyz Tien Shan granitoids (Central Asian Orogenic Belt): From emplacement to exhumation, *J. Asian Earth Sci.*, *38*(3–4), 131–146, doi:10.1016/j.jseaes.2009.12.009.

Goode, J. K., D. W. Burbank, and B. Bookhagen (2011), Basin width control of faulting in the Naryn Basin, South-central Tien Shan, *Tectonics*, doi:10.1029/2011TC002910.

Hardy, S., and J. Poblet (2005), A method for relating fault geometry, slip rate and uplift data above fault-propagation folds, *Basin Res.*, *17*(3), 417–424, doi:10.1111/J.1365-2117.2005.00268.X.

Heermance, R. V., J. Chen, D. W. Burbank, and C. S. Wang (2007), Chronology and tectonic controls of Late Tertiary deposition in the southwestern Tian Shan foreland, NW China, *Basin Res.*, doi:10.1111/j.1365-2117.2007.00339.x.

Hetzel, R., S. Niedermann, M. Tao, P. W. Kubik, S. Ivy-Ochs, B. Gao, and M. R. Strecker (2002), Low slip rates and long-term preservation of geomorphic features in Central Asia, *Nature*, *417*(6887), 428–432, doi:10.1038/417428a.

Hodges, K. V. (2000), Tectonics of the Himalaya and southern Tibet from two perspectives, *Geol. Soc. Am. Bull.*, *112*, 324–350.

Huang, M. H., J. C. Hu, C. S. Hsieh, K. E. Ching, R. J. Rau, E. Pathier, B. Fruneau, and B. Deffontaines (2006), A growing structure near the deformation front in SW Taiwan as deduced from SAR interferometry and geodetic observation, *Geophys. Res. Lett.*, *33*, L12305, doi:10.1029/2005GL025613.

Hubert-Ferrari, A., J. Suppe, R. Gonzalez-Mieres, and X. Wang (2007), Mechanisms of active folding of the landscape (southern Tian Shan, China), *J. Geophys. Res.*, *112*, B03S09, doi:10.1029/2006JB004362.

Huntley, D. J., D. I. Godfrey-Smith, and M. L. W. Thewalt (1985), Optical dating of sediments, *Nature*, *313*(5998), 105–107, doi:10.1038/313105a0.

Imbrie, J. (1984), The orbital theory of Pleistocene climate: Support from a revised chronology of the marine delta 18O record, in *Milankovitch and Climate*, edited by A. Berger, pp. 269–305, Reidel Publishing Company, Netherlands.

Karabanov, E. B., A. A. Prokopenko, D. F. Williams, and S. M. Colman (1998), Evidence from Lake Baikal for Siberian Glaciation during Oxygen-Isotope Substage 5d, *Quat. Res.*, *50*(1), 46–55, doi:10.1006/qres.1998.1980.

Korup, O., A. L. Strom, and J. T. Weidinger (2006), Fluvial response to large rock-slope failures: Examples from the Himalayas, the Tien Shan, and the Southern Alps in New Zealand, *Geomorphology*, *78*, 3–21, doi:10.1016/j.geomorph.2006.01.020.

Macaulay, E. A., E. R. Sobel, A. Mikolaichuk, A. Landgraf, B. Kohn, and F. Stuart (2013), Thermochronologic insight into Late Cenozoic deformation in the basement-cored Terskey Range, Kyrgyz Tien Shan, *Tectonics*, *32*, 475–500, doi:10.1002/tect.20040.

Makarov, V. I. (1977), *New Tectonic Structures of the Central Tien Shan* [in Russian], Order of the Red Banner Geology Institute, Academy of Science, Moscow.

Massonnet, D., M. Rossi, C. Carmona, F. Adragna, G. Peltzer, K. Feigl, and T. Rabaute (1993), The displacement of the Landers earthquake mapped by radar interferometry, *Nature*, *364*, 138–142.

Meade, B. J. (2007), Present-day kinematics at the India-Asia collision zone, *Geology*, *35*, 81–84.

Mellors, R. J., F. L. Vernohn, G. L. Pavlis, G. A. Abers, M. W. Hamburger, S. Ghose, and B. Illiasov (1997), The Ms = 7.3 1992 Suusamyr, Kyrgyzstan earthquake: 1. Contraints on fault geometry and source parameters based on aftershocks and body wave modeling, *Bull. Seismo. Soc. Am.*, *87*, 11–22.

Molnar, P., and S. Ghose (2000), Seismic moments of major earthquakes and the rate of shortening across the Tien Shan, *Geophys. Res. Lett.*, *27*, 2377–2380.
Murray, A. S., and A. G. Wintle (2000), Luminescence dating of quartz using an improved single-aliquot regenerative-dose protocol, *Radiat. Meas.*, *32*(1), 57–73, doi:10.1016/S1350-4487(99)00253-X.
Murray, A. S., and A. G. Wintle (2003), The single aliquot regenerative dose protocol: Potential for improvements in reliability, *Radiat. Meas.*, *37*(4–5), 377–381, doi:10.1016/S1350-4487(03)00053-2.
NASA and METI (2009), ASTER Global Digital Elevation Model, Jet Propul. Lab., Calif. Inst. of Technol., NASA, Pasadena, Calif. [Available at https://wist.echo.nasa.gov.]
Omuraliev, M. (1978), Geology and tectonic features of the Cenozoic Alabuga-Naryn Basin (central Tien Shan), PhD thesis, Inst. of Geophys. and Seismol., Acad. of Sci. of the Kirghiz SSR, Frunze, U.S.S.R.
Omuraliev, M. (1988), Geologic map of Cenozoic deposits Alabuga-Naryn Basin, scale 1:200,000.
Oskin, M. E., and D. W. Burbank (2007), Transient landscape evolution of basement-cored uplifts: Example of the Kyrgyz Range, Tian Shan, *J. Geophys. Res.*, *112*, F03S03, doi:10.1029/2006JF000563.
Oskin, M. E., D. W. Burbank, F. M. Phillips, S. M. Marrero, B. Bookhagen, and J. A. Selander (2014), Relationship of channel steepness to channel incision rate from a tilted and progressively exposed unconformity surface, *J. Geophys. Res. Earth Surf.*, doi:10.1002/2013JF002826.
Park, S. K., S. C. Thompson, A. Rybin, V. Batalev, and R. Bielinski (2003), Structural constraints in neotectonic studies of thrust faults from the magnetotelluric method, Kochkor Basin, Kyrgyz Republic, *Tectonics*, *22*(2), 1013, doi:10.1029/2001TC001318.
Peck, J. A., J. W. King, S. M. Colman, and V. A. Kravchinsky (1994), A rock-magnetic record from Lake Baikal, Siberia: Evidence for Late Quaternary climate change, *Earth Planet. Sci. Lett.*, *122*(1–2), 221–238.
Ramsey, C. B. (2009), Bayesian analysis of radiocarbon dates, *Radiocarbon*, *51*(1), 337–360.
Reigber, C., G. W. Michel, R. Galas, D. Angermann, J. Klotz, J. Y. Chen, A. Papschev, R. Arslanov, V. E. Tzurkov, and M. Ishanov (2001), New space geodetic constraints on the distribution of deformation in Central Asia, *Earth Planet. Sci. Lett.*, *191*, 157–165.
Reimer, P., et al. (2009), IntCal09 and Marine09 radiocarbon age calibration curves, 0–50,000 years cal BP, *Radiocarbon*, *51*(4), 1111–1150.
Robinson, D. M. D. (2001), The kinematic evolution of the Nepalese Himalaya interpreted from Nd isotopes, *Earth and Planet. Sci. Lett.*, *192*, 507–521.
Sengor, A. M. C., and B. A. Natal'in (1996), Turkic-type orogeny and its role in the making of the continental crust, *Ann. Rev. Earth Planet. Sci.*, *24*(1), 263–337, doi:10.1146/annurev.earth.24.1.263.
Shackleton, N. J. (2000), The 100,000-year ice-age cycle identified and found to lag temperature, carbon dioxide, and orbital eccentricity, *Science*, *289*(5486), 1897.
Sibson, R. H., and G. Xie (1998), Dip range for intracontinental reverse fault ruptures: Truth not stranger than friction?, *Bull. Seismol. Soc. Am.*, *88*, 1014–1022.
Sobel, E. R. (1999), Cenozoic exhumation of the Kyrgyz Tian Shan constrained by apatite fission track thermochronology, *Eos Trans.*, AGU Fall Meeting, *80*.
Sobel, E. R., J. Chen, and R. V. Heermance (2006a), Late Oligocene—Early Miocene initiation of shortening in the Southwestern Chinese Tian Shan: Implications for Neogene shortening rate variations, *Earth Planet. Sci. Lett.*, *247*, 70–81.
Sobel, E. R., E. A. Macaulay, A. Mikolaichuk, and B. P. Kohn (2008), Late Cenozoic Exhumation of the Terskey Range, Kyrgyz Tien Shan, *EOS Trans.*, supplement: Fall meeting Abstracts, Abstract T53A-1907.
Sobel, E. R., M. Oskin, D. W. Burbank, and A. Mikolaichuk (2006b), Exhumation of basement-cored uplifts: Example of the Kyrgyz Range quantified with apatite fission-track thermochronology, *Tectonics*, *25*, TC2008, doi:10.1029/2005TC001809.
Strom, A. L., and O. Korup (2006), Extremely large rockslides and rock avalanches in the Tien Shan Mountains, Kyrgyzstan, *Landslides*, *3*(2), 125–136, doi:10.1007/s10346-005-0027-7.
Suppe, J., G. T. Chou, and S. C. Hook (1992), Rates of folding and faulting determined from growth strata, in *Thrust Tectonics*, vol. 1, edited by K. R. McClay, pp. 105–121, Chapman & Hall, Suffolk.
Suppe, J., and D. A. Medwedeff (1990), Geometry and kinematics of fault-propagation folding, *Eclogae Geol. Helv.*, *83*(3), 409–454.
Tapponnier, P., and P. Molnar (1979), Active faulting and Cenozoic tectonics of the Tien Shan, Mongolia, and Baykal regions, *J. Geophys. Res.*, *84*(B7), 3425–3459.
Thompson, S. C., R. Weldon, C. M. Rubin, K. Y. Abdrakhmatov, P. Molnar, and G. W. Berger (2002), Late Quaternary slip rates across the central Tien Shan, Kyrgyzstan, central Asia, *J. Geophys. Res.*, *107*(B9), 2203, doi:10.1029/2001JB000596.
Windley, B. F., D. Alexeiev, W. Xiao, A. Kroner, and G. Badarch (2007), Tectonic models for accretion of the Central Asian Orogenic Belt, *J. Geol. Soc. London*, *164*, 31–47, doi:10.1144/0016-76492006-022.
Wright, T. J., B. Parsons, P. C. England, and E. J. Fielding (2004), InSAR observations of low slip rates on the major faults of western Tibet, *Science*, *305*(5681), 236–239, doi:10.1126/science.1096388.
Yin, A., S. Nie, P. Craig, T. M. Harrison, F. J. Ryerson, Q. Xianglin, and Y. Geng (1998), Late Cenozoic tectonic evolution of the southern Chinese Tien Shan, *Tectonics*, *17*(1), 1–27.
Zubovich, A. V., et al. (2010), GPS velocity field for the Tien Shan and surrounding regions, *Tectonics*, *29*, TC6014, doi:10.1029/2010TC002772.